Bending-induced mode non-degeneracy and coupling in chalcogenide negative curvature fibers

Chengli Wei,[1] Curtis R. Menyuk,[2] and Jonathan Hu[1,*]

[1]*Baylor University, One Bear Place #97356, Waco, TX, 76798 USA*

[2]*University of Maryland Baltimore County, 5200 Westland Blvd., Baltimore, MD, 21227 USA*

[*] *Jonathan_hu@baylor.edu*

Abstract: We study bend loss in chalcogenide negative curvature fibers with different polarizations, different tube wall thicknesses, and different bend directions relative to the mode polarization. The coupling between the core mode and tube modes induces bend loss peaks in the two non-degenerate modes at the same bend radius. There is as much as a factor of 28 difference between the losses of the two polarization modes. The fiber with a larger tube wall thickness, corresponding to a smaller inner tube diameter, can sustain a smaller bend radius. The bend loss is sensitive to the bend direction when coupling occurs between the core mode and tube modes. A bend loss of 0.2 dB/m at a bend radius of 16 cm, corresponding to 0.2 dB/turn, can be achieved in a chalcogenide negative curvature fiber.

OCIS codes: (060.2280) Fiber design and fabrication; (060.2400) Fiber properties; (060.2390) Fiber optics, infrared.

References and links

1. J. Broeng, S. E. Barkou, T. Søndergaard, and A. Bjarklev, "Analysis of air-guiding photonic bandgap fibers," Opt. Lett. **25**(2), 96–98 (2000).
2. G. Pearce, J. Pottage, D. Bird, P. Roberts, J. Knight, and P. Russell, "Hollow-core PCF for guidance in the mid to far infra-red," Opt. Express **13**(18), 6937–6946 (2005).
3. J. Hu and C. R. Menyuk, "Leakage loss and bandgap analysis in air-core photonic bandgap fiber for nonsilica glasses," Opt. Express **15**(2), 339–349 (2007).
4. P. Russell, "Photonic-crystal fibers," J. Lightwave Technol. **24**(12), 4729–4749 (2006).
5. J. C. Knight, J. Broeng, T. A. Birks, and P. S. J. Russell, "Photonic band gap guidance in optical fibers," Science **282**(5393), 1476–1478 (1998).
6. A. D. Pryamikov, A. S. Biriukov, A. F. Kosolapov, V. G. Plotnichenko, S. L. Semjonov, and E. M. Dianov, "Demonstration of a waveguide regime for a silica hollow-core microstructured optical fiber with a negative curvature of the core boundary in the spectral region $> 3.5\ \mu$m," Opt. Express **19**(2), 1441–1448 (2011).
7. F. Yu, W. J. Wadsworth, and J. C. Knight, "Low loss silica hollow core fibers for 3–4 μm spectral region," Opt. Express **20**(10), 11153–11158 (2012).
8. A. N. Kolyadin, A. F. Kosolapov, A. D. Pryamikov, A. S. Biriukov, V. G. Plotnichenko, and E. M. Dianov, "Light transmission in negative curvature hollow core fiber in extremely high material loss region," Opt. Express **21**(8), 9514–9519 (2013).
9. F. Yu and J. C. Knight, "Spectral attenuation limits of silica hollow core negative curvature fiber," Opt. Express **21**(18), 21466–21471 (2013).
10. W. Belardi and J. C. Knight, "Hollow antiresonant fibers with reduced attenuation," Opt. Lett. **39**(7), 1853–1856 (2014).
11. W. Ding and Y. Wang, "Hybrid transmission bands and large birefringence in hollow-core anti-resonant fibers," Opt. Express **23**(16), 21165–21174 (2015).

#263392 Received 19 Apr 2016; revised 18 May 2016; accepted 19 May 2016; published 26 May 2016

12. A. Hartung, J. Kobelke, A. Schwuchow, K. Wondraczek, J. Bierlich, J. Popp, T. Frosch, and M. A. Schmidt, "Double antiresonant hollow core fiber-guidance in the deep ultraviolet by modified tunneling leaky modes," Opt. Express **22**(19), 19131–19140 (2014).
13. W. Belardi and J. C. Knight, "Effect of core boundary curvature on the confinement losses of hollow antiresonant fibers," Opt. Express **21**(19), 21912–21917 (2013).
14. P. Jaworski, F. Yu, R. R. J. Maier, W. J. Wadsworth, J. C. Knight, J. D. Shephard, and D. P. Hand, "Picosecond and nanosecond pulse delivery through a hollow-core negative curvature fiber for micro-machining applications," Opt. Express **21**(19), 22742–22753 (2013).
15. A. Urich, R. R. J. Maier, F. Yu, J. C. Knight, D. P. Hand, and J. D. Shephard, "Flexible delivery of Er:YAG radiation at 2.94 μm with negative curvature silica glass fibers: a new solution for minimally invasive surgical procedures," Biomed. Opt. Express **4**(2), 193–205 (2013).
16. Y. Wang, F. Couny, P. J. Roberts, and F. Benabid, "Low loss broadband transmission in optimized core-shaped Kagome hollow-core PCF," in *Conference on Lasers and Electro-Optics/Quantum Electronics and Laser*, Post-deadline Papers (Optical Society of America, 2010), paper CPDB4.
17. Y. Y. Wang, N. V. Wheeler, F. Couny, P. J. Roberts, and F. Benabid, "Low loss broadband transmission in hypocycloid-core Kagome hollow-core photonic crystal fiber," Opt. Lett. **36**(5), 669–671 (2011).
18. A. F. Kosolapov, A. D. Pryamikov, A. S. Biriukov, V. S. Shiryaev, M. S. Astapovich, G. E. Snopatin, V. G. Plotnichenko, M. F. Churbanov, and E. M. Dianov, "Demonstration of CO_2-laser power delivery through chalcogenide-glass fiber with negative-curvature hollow core," Opt. Express **19**(25), 25723–25728 (2011).
19. V. S. Shiryaev, A. F. Kosolapov, A. D. Pryamikov, G. E. Snopatin, M. F. Churbanov, A. S. Biriukov, T. V. Kotereva, S. V. Mishinov, G. K. Alagashev, and A. N. Kolyadin, "Development of technique for preparation of As_2S_3 glass preforms for hollow core microstructured optical fibers," J. Optoelectron. Adv. M. **16**(9–10), 1020–1025 (2014).
20. V. S. Shiryaev, "Chalcogenide glass hollow-core microstructured optical fibers," Front. Mater. **2**(24), (2015).
21. D. D. Hudson, E. C. Mägi, A. C. Judge, S. A. Dekker, and B. J. Eggleton, "Highly nonlinear chalcogenide glass micro/nanofiber devices: Design, theory, and octave-spanning spectral generation," Opt. Commun. **285**(23), 4660–4669 (2012).
22. F. K. Tittel, D. Richter, and A. Fried, "Mid-infrared laser applications in spectroscopy," in *Solid-State Mid-Infrared Laser Sources*, I.T. Sorokina and K.L. Vodopyanov, ed. (Springer, 2003).
23. A. Schliesser, N. Picqué, and T. W. Hänsch, "Mid-infrared frequency combs," Nat. Photonics **6**(7), 440–449 (2012).
24. Y. Bai, S. Slivken, S. Kuboya, S. R. Darvish, and M. Razeghi, "Quantum cascade lasers that emit more light than heat," Nat. Photonics **4**(2), 99–102 (2010).
25. P. Q. Liu, A. J. Hoffman, M. D. Escarra, K. J. Franz, J. B. Khurgin, Y. Dikmelik, X. Wang, J.-Y. Fan, and C. F. Gmachl, "Highly power-efficient quantum cascade lasers," Nat. Photonics **4**(2), 95–98 (2010).
26. Y. Yao, J. A. Hoffman, and C. F. Gmachl, "Mid-infrared quantum cascade lasers," Nat. Photonics **6**(7), 432–439 (2012).
27. Y. Bai, N. Bandyopadhyay, S. Tsao, S. Slivken and M. Razeghi, "Room temperature quantum cascade lasers with 27% wall plug efficiency," Appl. Phys. Lett. **98**(18), 181102 (2011).
28. J. Hu, C. R. Menyuk, L. B. Shaw, J. S. Sanghera, and I. D. Aggarwal, "Computational study of a 3–5 μm source that is created by using supercontinuum generation in As_2S_3 chalcogenide fibers with a pump at 2 μm," Opt. Lett. **35**(17), 2907–2909 (2010).
29. J. Hu and C. R. Menyuk, "Understanding leaky modes: slab waveguide revisited," Adv. Opt. Photonics **1**(1), 58–106 (2009).
30. C. Wei, R. A. Kuis, F. Chenard, C. R. Menyuk, and J. Hu, "Higher-order mode suppression in chalcogenide negative curvature fibers," Opt. Express **23**(12), 15824–15832 (2015).
31. A. Hartung, J. Kobelke, A. Schwuchow, J. Bierlich, J. Popp, M. A. Schmidt, and T. Frosch, "Low-loss single-mode guidance in large-core antiresonant hollow-core fibers," Opt. Lett. **40**(14), 3432–3435 (2015).
32. M. S. Habib, O. Bang, and M. Bache, "Low-loss hollow-core silica fibers with adjacent nested anti-resonant tubes," Opt. Express **23**(13), 17394–17406 (2015).
33. M. S. Habib, O. Bang, and M. Bache, "Low-loss single-mode hollow-core fiber with anisotropic anti-resonant elements," Opt. Express **24**(8), 8429–8436 (2016).
34. P. Uebel, M. Günendi, M. H. Frosz, G. Ahmed, N. Edavalath, J. Ménard, and P. S. Russell, "A broad-band robustly single-mode hollow-core PCF by resonant filtering of higher order modes," in *Frontiers in Optics 2015*, OSA Technical Digest (online) (Optical Society of America, 2015), paper FW6C.2.
35. P. Uebel, M. C. Günendi, M. H. Frosz, G. Ahmed, N. N. Edavalath, J.-M. Ménard, and P. S. J. Russell, "Broad-band robustly single-mode hollow-core PCF by resonant filtering of higher-order modes," Opt. Lett. **41**(14), 1961–1964 (2016).
36. F. Poletti, "Nested antiresonant nodeless hollow core fiber," Opt. Express **22**(20), 23807–23828 (2014).
37. C. Wei, J. Hu, and C. Menyuk, "Bending-induced mode coupling in chalcogenide negative curvature fibers," in *Advanced Photonics 2015*, OSA Technical Digest (online) (Optical Society of America, 2015), paper NT2C.5.
38. W. Belardi and J. C. Knight, "Hollow antiresonant fibers with low bending loss," Opt. Express **22**(8), 10091–

#263392 Received 19 Apr 2016; revised 18 May 2016; accepted 19 May 2016; published 26 May 2016

10096 (2014).
39. V. Setti, L. Vincetti, and A. Argyros, "Flexible tube lattice fibers for terahertz applications," Opt. Express **21**(3), 3388–3399 (2013).
40. A. D. Pryamikov, A. F. Kosolapov, V. G. Plotnichenko, and E. M. Dianov, "Transmission of CO_2 Laser Radiation through glass hollow core microstructured fibers," in *CO_2 Laser - Optimisation and Application*, D. C. Dumitras, ed. (InTech, 2012).
41. M. Michieletto, J. K. Lyngsø, C. Jakobsen, J. Lægsgaard, O. Bang, and T. T. Alkeskjold, "Hollow-core fibres for high power pulse delivery," Opt. Express **24**(7), 7103–7119 (2016).
42. M. Alharbi, T. Bradley, B. Debord, C. Fourcade-Dutin, D. Ghosh, L. Vincetti, F. Gérôme, and F. Benabid, "Hypocycloid-shaped hollow-core photonic crystal fiber Part II: Cladding effect on confinement and bend loss," Opt. Express **21**(23), 28609–28616 (2013).
43. G. K. Alagashev, A. D. Pryamikov, A. F. Kosolapov, A. N. Kolyadin, A. Yu. Lukovkin, and A. S. Biriukov, "Impact of geometrical parameters on the optical properties of negative curvature hollow core fibers," Laser Phys. **25**(5), 055101 (2015).
44. K. Saitoh and M. Koshiba, "Leakage loss and group velocity dispersion in air-core photonic bandgap fibers," Opt. Express **11**(23), 3100–3109 (2003).
45. G. Ren, Z. Wang, S. Lou, and S. Jian, "Mode classification and degeneracy in photonic crystal fibers," Opt. Express **11**(11), 1310–1321 (2003).
46. M. Heiblum and J. H. Harris, "Analysis of curved optical waveguides by conformal transformation," IEEE J. Quantum Electron. **11**(2), 75–83 (1975).
47. M. A. Duguay, Y. Kokubun, T. L. Koch, and L. Pfeiffer, "Antiresonant reflecting optical waveguides in SiO_2-Si multilayer structures," Appl. Phys. Lett. **49**(13), 13–15 (1986).
48. N. M. Litchinitser, A. K. Abeeluck, C. Headley, and B. J. Eggleton, "Antiresonant reflecting photonic crystal optical waveguides," Opt. Lett. **27**(18), 1592–1594 (2002).
49. W. Ding and Y. Wang, "Analytic model for light guidance in single-wall hollow-core anti-resonant fibers," Opt. Express **22**(22), 27242–27256 (2014).
50. W. Liu, T. Guo, A. C. Wong, H. Y. Tam, and S. He, "Highly sensitive bending sensor based on Er^{3+}-doped DBR fiber laser," Opt. Express **18**(17), 17834–17840 (2010).
51. M. Deng, C. P. Tang, T. Zhu, and Y. J. Rao, "Highly sensitive bend sensor based on Mach-Zehnder interferometer using photonic crystal fiber," Opt. Commun. **284**(12), 2849–2853 (2011).

1. Introduction

Hollow-core photonic crystal fibers have the potential to provide low-loss transmission, along with delivery of high-power light with low nonlinearity. A photonic bandgap structure uses a periodic array of air holes in the cladding to confine light in the core [1–5]. In recent years, hollow-core negative curvature fibers using the antiresonance guiding mechanism have drawn much attention due to their attractive fiber properties that include a low transmission loss, a simple structure, and a wide transmission bandwidth [6–17]. Negative curvature implies that the surface normal to the core boundary is oppositely directed from the core. Since no bandgap is used, there is no requirement for a periodic cladding structure. The use of chalcogenide fibers in fiber devices that require a periodic structure has been hampered by fabrication difficulties [18–21].

The relative simplicity of the negative curvature structure could enable the fabrication of fiber devices for mid-IR applications using non-silica glasses, such as chalcogenide. Using chalcogenide negative curvature fibers, the delivery of mid-infrared radiation has been successfully demonstrated for a CO_2 laser at a wavelength of 10.6 μm [18]. Mid-infrared light sources and transmission are important for applications to biosensing, environmental monitoring, homeland security, and medical diagnostics [22, 23]. The development of quantum cascade lasers has shown great potential for the generation of mid-infrared emission around 5 μm with a wall plug efficiency of 50% [24–26] and a watt-level power output [27]. While transmission of light in silica negative curvature fibers has been demonstrated at wavelengths up to 4 μm [9], the material loss of chalcogenide glass is four orders of magnitude or more lower than silica glass at wavelengths at or above 5 μm [8, 28]. So, it is preferable to use chalcogenide glass at these wavelengths.

In negative curvature fibers, core sizes from 20 μm to 380 μm have been used [6–18]. Fibers

#263392 Received 19 Apr 2016; revised 18 May 2016; accepted 19 May 2016; published 26 May 2016

with a large core size have a low leakage loss [29]. At the same time, fibers with a large core size have many higher-order modes [30]. Several structures have been suggested to suppress higher-order modes using the resonant coupling between the higher-order core modes and cladding modes [30–36]. Another important limiting factor in fiber devices is the bend loss. Bend effectively introduces structure distortion, especially for fibers with a large core cross section [37–40]. It is preferable for a fiber to insensitive to bends when it is used for light delivery. Conversely, however, bend sensitivity can be useful for sensing. In bandgap fibers, since the cladding air holes are much smaller than the central air core, there is not much loss due to the mode coupling between the core modes and the cladding modes. The bend loss for a bandgap fiber is mainly due to distortion of the fiber structure. In negative curvature fibers, besides the structure's distortion, the mode coupling between the core mode and tube modes leads to an increase in the loss of the core modes. Bending-induced higher-order mode suppression has been obtained using the resonant coupling between the higher-order core modes and the tube modes in negative curvature fibers [41]. Structures that include nested cladding tubes or smaller cladding tubes have also been proposed to decrease the bend loss [36, 38]. To date, there is no detailed study on two polarization modes in bent negative curvature fibers [33, 36–40, 42, 43]. In this paper, we study the bending-induced mode coupling for the non-degenerate core modes in chalcogenide negative curvature fibers. Fiber bends break the symmetry of the fiber geometry, and the fundamental core modes become non-degenerate modes in bent negative curvature fibers. It is thus necessary to take into account the mode polarization when calculating the loss in bent fibers. We find that the loss in the two polarization modes can differ by up to a factor of 28.

The rest of the paper is organized as follows: In section 2, we show the fiber geometry. We also present the bend loss for both parallel-polarized and perpendicular-polarized modes with respect to the bend direction in the chalcogenide negative curvature fiber. In section 3, we study the avoided crossing during the resonant coupling between the core mode and the tube modes. Two non-degenerate core modes can be coupled to tube modes at the same bend radius. In section 4, we study the influence from the tube wall thickness on the resonant coupling. We find that a fiber with a larger tube wall thickness, corresponding to a smaller inner tube diameter, can sustain a smaller bend radius. In section 5, we study the bend loss when the relative angle between the bend direction and fiber orientation varies, since the bend direction is not always aligned with the fiber geometry in practice. The bend loss is sensitive to the bend direction when coupling occurs between the core mode and a tube mode. We summarize our results in section 6.

2. Geometry and bend loss

In this section, we introduce the geometric parameters of the negative curvature fiber. Figure 1 shows the full hollow-core negative curvature fiber geometry. The gray regions represent glass, and the white regions represent air. The inner tube diameter, d_{tube}, the core diameter, D_{core}, the tube wall thickness, t, and the minimum gap between the cladding tubes, g, are related by the expression: $D_{\text{core}} = (d_{\text{tube}} + 2t + g)/\sin(\pi/8) - (d_{\text{tube}} + 2t)$. The core diameter, D_{core}, and the gap, g, are fixed at 150 μm and 10 μm, respectively. The wavelength is 5 μm in our simulation. Negative curvature fibers have been drawn using 6 or 8 cladding tubes [6, 8, 18–20, 35, 43]. We use 8 cladding tubes in this paper because negative curvature fibers with a smaller cladding tube diameter yield a lower bend loss [38].

We calculate the fiber modes and their propagation constants using Comsol Multiphysics, a commercial full-vector mode solver based on the finite-element method. Anisotropic, perfectly matched layers (PMLs) are positioned outside the cladding in order to reduce the size of the simulation window [44]. We simulate As_2S_3 chalcogenide glass with a refractive index whose

#263392 Received 19 Apr 2016; revised 18 May 2016; accepted 19 May 2016; published 26 May 2016

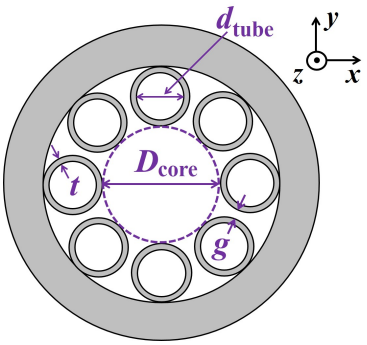

Fig. 1. Cross section of a chalcogenide negative curvature fiber.

real part equals 2.4 and whose imaginary part equals 3.4×10^{-8} [28].

We studied the bend loss using the above negative curvature fiber geometry. We assume that the bend is along the x-axis, and we take advantage of the reflection symmetry with respect to the $y = 0$ plane to only keep values for which $y > 0$ in the simulation [45]. A conformal transformation is used to replace the bent fiber with a straight fiber that has an equivalent index distribution: $n'(x,y) = n(x,y)\cdot\exp(x/R)$, where R is the bend radius [37,46]. Figures 2(a) and 2(b) show the contour plot of the bend loss as a function of bend radius and tube wall thickness for the fundamental core modes that are polarized parallel and perpendicular to the bend direction, respectively. We observe that losses are consistently high for the tube wall thicknesses, t = 1.15 μm, 2.29 μm, and 3.44 μm, that satisfy the resonance condition, $t = m\lambda/[2(n_1^2 - n_0^2)^{1/2}]$, where n_1 and n_0 are respectively the real parts of the refractive indices of the glass and air [47–49]. We observe three transmission bands, I, II, and III, which are separated by the above tube wall thicknesses in both Figs. 2(a) and 2(b). In the following sections, we will study the bend loss with different polarizations, different tube wall thicknesses, and different bend directions.

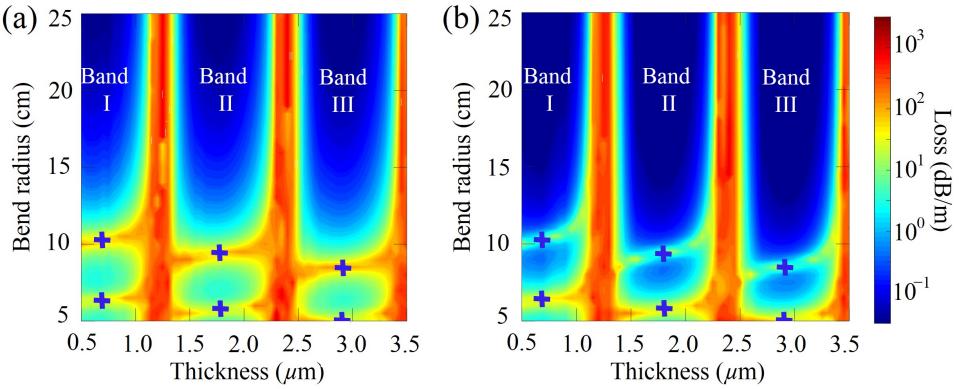

Fig. 2. Bend loss of the fundamental mode that is polarized (a) parallel and (b) perpendicular to the bend direction as a function of the tube wall thickness and the bend radius. The plus signs denote points at which the loss becomes high relative to the bend-free loss even though the thickness is antiresonant.

#263392 Received 19 Apr 2016; revised 18 May 2016; accepted 19 May 2016; published 26 May 2016

3. Modes in two polarizations

In this section, we will compare the bend loss in two fundamental modes whose polarization directions are parallel or perpendicular to the bend direction. The tube wall thickness is fixed at 1.8 μm. Figure 3(a) shows the real parts of the effective indices of the parallel-polarized and perpendicular-polarized core modes, as the blue dashed curve and red solid curve, respectively. We can see that there are two avoided crossings at bend radii of 5.7 cm and 9.4 cm, and the index difference between the two polarized core modes is very small. Figure 3(b) shows the bend losses for core modes at different bend radii. There are two high loss peaks in the bend loss curves for both the parallel-polarized and perpendicular-polarized modes, which are consistent with the two avoided crossings shown in Fig. 3(a).

The mode structure at the two bend-loss peaks is different. Figure 4 shows both the parallel-polarized and perpendicular-polarized modes at bend radii of 5.7 cm and 9.4 cm, corresponding to the avoided crossings and the loss peaks in Fig. 3. We only show the mode in the middle of the avoided crossing; the evolution of the mode during the avoided crossing has been described in negative curvature fibers with 8 cladding tubes [30]. The color indicates the electric field intensity, normalized to its maximum. The arrows indicate the direction of the transverse electric

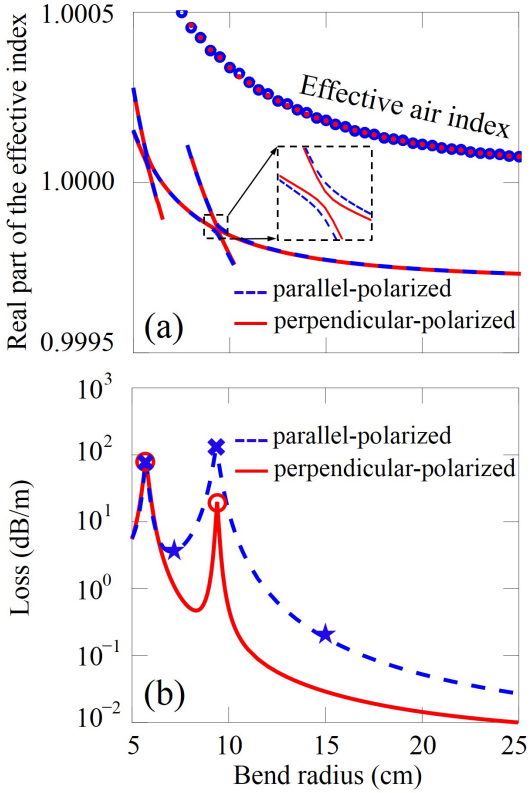

Fig. 3. (a) Real parts of the effective indices and (b) bend losses for both parallel-polarized and perpendicular-polarized modes in the negative curvature fiber with a tube wall thickness of 1.8 μm. The inset shows the avoided crossing close to a bend radius of 9.4 cm. The effective air index is defined as the index after conformal transformation at the peak of the core mode intensity.

#263392 Received 19 Apr 2016; revised 18 May 2016; accepted 19 May 2016; published 26 May 2016

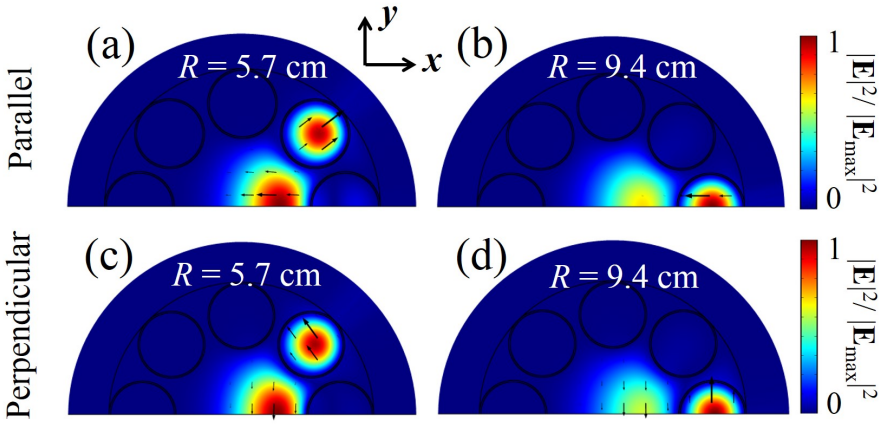

Fig. 4. The parallel-polarized and perpendicular-polarized modes at bend radii of 5.7 cm and 9.4 cm. The contour plots represent the normalized electric field intensity, and the arrows represent the amplitude and direction of the transverse electric field.

field and the lengths of the arrows are proportional to the amplitude of the transverse electric field. We can see that, at a bend radius of 9.4 cm, coupling occurs between the core mode and the tube mode, which is located along the bend direction, as indicated by Figs. 4(b) and 4(d). The bend loss of the parallel-polarized mode is higher than the bend loss of the perpendicular-polarized mode as shown in Fig. 3(b). The alignment of the core mode and the coupled tube mode is the same as the polarization direction for the parallel-polarized mode. Therefore, the coupling is stronger for the parallel-polarized mode and leads to a loss that is up to a factor of 6 higher than the loss of the perpendicular-polarized mode when the bend radius is 15 cm and is up to a factor of 28 higher when the bend radius is 10 cm. Since both parallel-polarized and perpendicular-polarized core modes are coupled to the same tube modes, avoided crossings and loss peaks occur at the same bend radius, as indicated by Fig. 3. At a smaller bend radius of 5.7 cm, the index in the tube along the bend direction is higher than the core index. Index matching occurs between the core mode and the tube mode in the tube at 45 degree with respect to bend direction or x-axis [39], as indicated by Figs. 4(a) and 4(c). In addition, since both the core modes in the two polarizations are coupled to the tube mode at 45 degree with respect to their polarization directions, those two non-degenerate modes have almost the same loss at the bend radius of 5.7 cm, as shown in Fig. 3(b).

In Fig. 5, we show the parallel-polarized modes at bend radii of 7.0 cm and 15.0 cm, corresponding to the two stars in Fig. 3(b). The modes are well-confined in the core. Conversely,

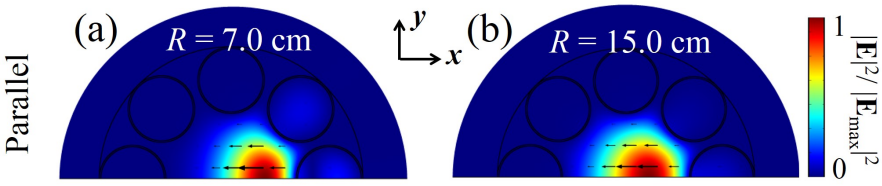

Fig. 5. The parallel-polarized fundamental core modes at bend radii of (a) 7.0 cm and (b) 15.0 cm.

#263392 Received 19 Apr 2016; revised 18 May 2016; accepted 19 May 2016; published 26 May 2016

coupling between the core and tube mode at the bend radius of 9.4 cm is visible in Fig. 4(b). Hence, the bend loss peaks in Fig. 3(b) are indeed induced by the mode coupling between the core and tube modes in the negative curvature fiber [30, 38].

We also note that some of the mode effective indices are higher than the refractive index (n = 1.0), which is due to the fiber bend. Figure 3(a) shows the effective air indices for the parallel-polarized and perpendicular-polarized modes as blue open circles and red dots, respectively. The effective air index is defined as the index after conformal transformation at the peak of the core mode intensity. The peak of the core mode intensity is not at the center of the core in the bent fiber, as shown in Fig. 5. Hence, the modes indicated by the blue dashed curve and the red solid curve in Fig. 3(a) have effective indices that are below the effective air index and are the fundamental core modes confined in the air core of the negative curvature fiber.

4. Different tube thicknesses

In Figs. 2(a) and 2(b), we see that besides the high loss that occurs at resonant tube thicknesses, there are in addition bend radii that lead to high loss, which are denoted by plus signs. In this section, we study these bend loss peaks for a fiber with different tube thicknesses [37]. In order to analyze the source of these high loss ranges, Figs. 6(a) and 6(b) show the real parts of the effective indices and bend losses, respectively, for the parallel-polarized mode with fixed tube wall thicknesses of 0.7 μm, 1.8 μm, and 2.9 μm. We present results for the parallel-polarized

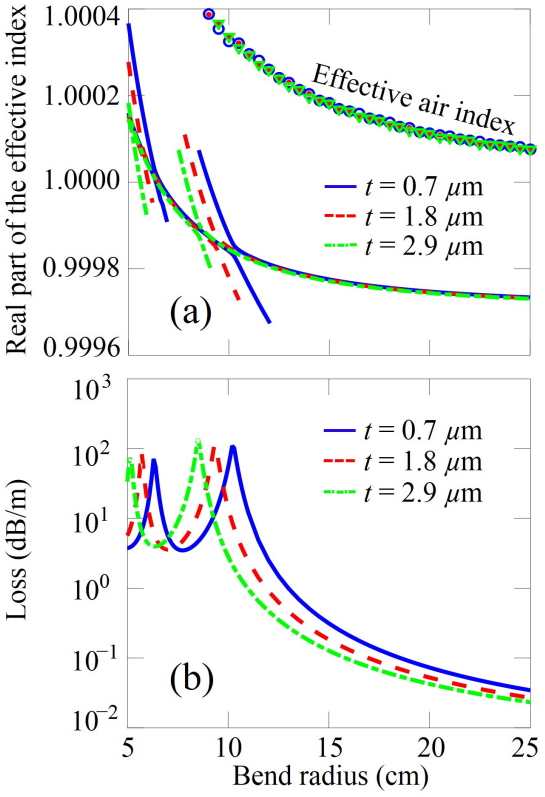

Fig. 6. (a) Real parts of the effective indices and (b) bend losses for the parallel-polarized mode with tube wall thicknesses of 0.7 μm, 1.8 μm, and 2.9 μm.

#263392 Received 19 Apr 2016; revised 18 May 2016; accepted 19 May 2016; published 26 May 2016

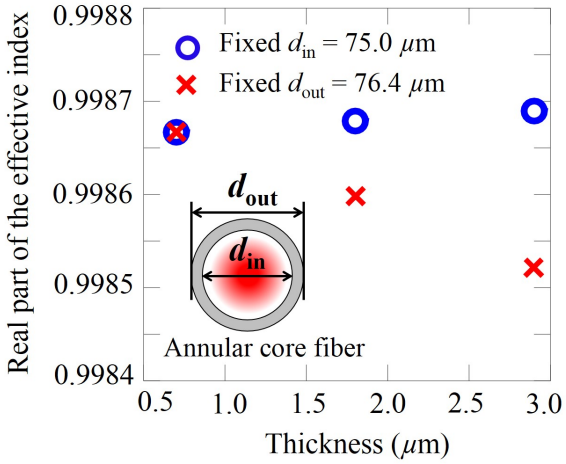

Fig. 7. Real parts of the effective indices in annular core fibers with a fixed inner tube diameter or a fixed outer tube diameter. The inset shows the geometry of an annular core fiber.

mode because it has a larger leakage loss than does the perpendicular-polarized mode. The real part of the effective index for the perpendicular-polarized mode is essentially the same as that for the parallel-polarized mode, and the bend loss exhibits peaks at the same bend radii as the parallel-polarized mode, although the loss peaks are lower. The avoided crossings are visible in Fig. 6(a). The loss peaks in Fig. 6(b) correspond to the high loss ranges in Fig. 2(a) that are marked by the plus signs. Note that the peak of the bend loss for fibers with a larger tube wall thickness occurs at a smaller bend radius, as shown in Fig. 6(b).

Mode coupling occurs when the effective indices of the core and tube modes match. In order to explain the results in Fig. 6, we study both the core mode and the tube modes when the tube wall thickness increases. The effective indices of the core modes with the same core diameter are almost the same even with different tube wall thicknesses. To predict the effective index of the tube mode, we ran additional simulations to find the mode in an annular core fiber [30], which contains just one ring of glass, as shown in Fig. 7. We study annular core fibers in two cases. For the first case, we use tube wall thicknesses of 0.7 μm, 1.8 μm, and 2.9 μm with a fixed inner tube diameter d_{in} of 75 μm. For the second case, we use tube wall thicknesses of 0.7 μm, 1.8 μm, and 2.9 μm with a fixed outer tube diameter d_{out} of 76.4 μm. The tube parameters of an inner tube diameter d_{in} of 75 μm and an outer tube diameter d_{out} of 76.4 μm correspond to the tube parameters in a straight negative curvature fiber using a core diameter of 150 μm, a tube wall thickness of 0.7 μm, and a minimum gap between the cladding tubes of 10 μm. In a fiber with a fixed inner tube diameter of 75 μm, the effective index increases slightly when the tube wall thickness increases from 0.7 μm to 2.9 μm. In a fiber with a fixed outer tube diameter of 76.4 μm, the effective index decreases when the tube wall thickness increases from 0.7 μm to 2.9 μm. Hence, if one increases the tube wall thickness while the outer diameter of the tubes is fixed in a negative curvature fiber, the effective index of the tube mode decreases because the inner diameter of the tubes decreases. Bending effectively increases the effective index of certain tube modes. Hence, the avoided crossing and mode coupling occur at a smaller bend radius for the fiber with a larger tube wall thickness, corresponding to a smaller inner tube diameter, as shown in Figs. 6(a) and 6(b). This finding is consistent with research on negative curvature fibers in which more tubes are used [38]. The corresponding effective air indices in the fibers with tube wall thicknesses of 0.7 μm, 1.8 μm, and 2.9 μm are shown in Fig. 6(a) by

#263392 Received 19 Apr 2016; revised 18 May 2016; accepted 19 May 2016; published 26 May 2016

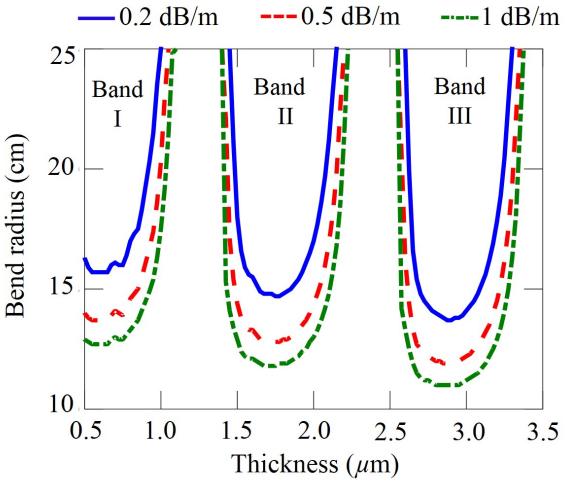

Fig. 8. Minimum bend radius for the parallel-polarized mode as a function of tube wall thickness for given bend losses of 0.2 dB/m, 0.5 dB/m and 1.0 dB/m.

blue circles, red dots and green triangles, respectively.

From Fig. 2(a), we can infer the minimum bend radius for a given loss. We then plot the minimum bend radius with respect to the tube wall thickness for given bend losses of 0.2 dB/m, 0.5 dB/m, and 1 dB/m for the parallel-polarized mode in Fig. 8. We again observe three transmission bands. As expected, a smaller loss requires a larger bend radius. The minimum bend radius for any given bend loss decreases as the transmission-band order increases in the parameter range we study here. Hence, a negative curvature fiber with a larger tube wall thickness can sustain a smaller bend radius. The reason is that the mode coupling in the fiber with a larger tube wall thickness, corresponding to a smaller inner tube diameter, occurs at a smaller bend radius, as we explained earlier. The bend loss is less than 0.2 dB/m in the transmission bands I, II, and III, corresponding to a loss value of 0.2 dB/turn if the fiber has a bend radius of 16 cm.

5. Different bend directions

Our previous simulations assumed that the bend direction is aligned with x-direction, as shown in Fig. 1 [10, 37, 38]. In practice, the bend can be in any direction. In this section, we will consider a bend direction with a relative angle, $\Delta\theta$, with respect to the x-direction. Since symmetry is broken, a full fiber geometry model has to be used in the simulation. The tube wall thickness is 1.8 μm. Figure 9(a) shows the bend losses for the two fundamental core modes as a function of the relative angle with respect to the x-axis at a bend radius of 9.4 cm, where the resonant coupling occurs. The loss is symmetrical about a bend relative angle of $\pi/8$ due to the fiber symmetry. When the bend relative angle changes from 0 to $\pi/8$, the leakage loss of the parallel-polarized mode, indicated by the blue dashed curve, and the perpendicular-polarized mode, indicated by the red solid curve, decrease by factors of 12 and 10, respectively. When the bend relative angle changes from 0 to $\pi/8$, the mode changes from being resonantly coupled to being slightly off resonance. Hence, the index matching condition is strongly affected by the relative angle, which leads to a large variation in the loss as the bend relative angle varies. The parallel-polarized mode profiles at relative angles of 0 and $\pi/8$ are shown in Figs. 10(a) and 10(c), respectively, at a bend radius of 9.4 cm. We see that the coupling between the core mode and tube mode is strong at $\Delta\theta = 0$, and the coupling between the core mode and tube mode is weak at $\Delta\theta = \pi/8$.

#263392 Received 19 Apr 2016; revised 18 May 2016; accepted 19 May 2016; published 26 May 2016

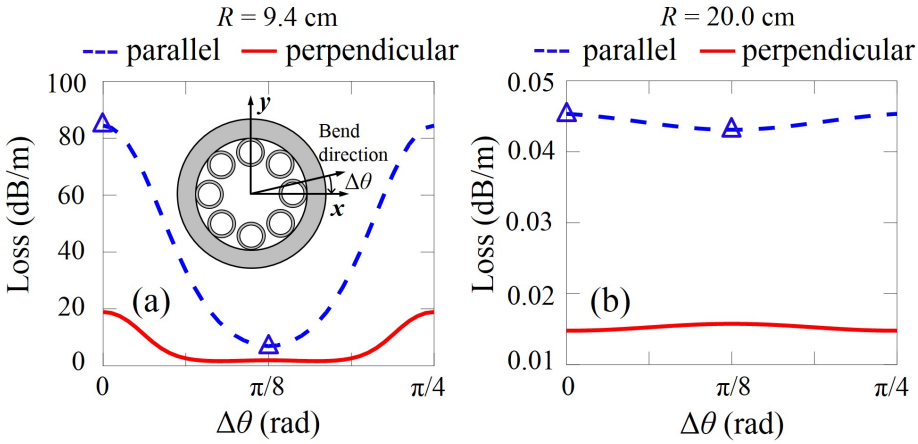

Fig. 9. Bend losses of the parallel-polarized and perpendicular-polarized modes as a function of bend relative angle for the fibers with a tube wall thickness of 1.8 μm at bend radii of (a) 9.4 cm and (b) 20.0 cm. The inset shows the relative angle, $\Delta\theta$, between the bend direction and x-axis in the negative curvature fiber. The blue triangles mark the relative angles for the mode fields that are shown in Fig. 10.

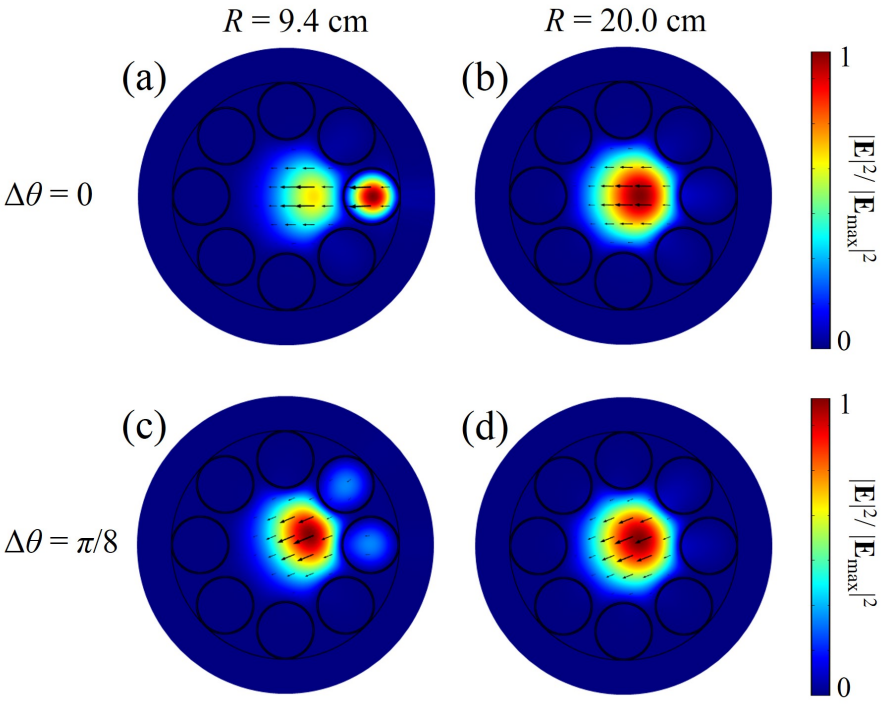

Fig. 10. Parallel-polarized core mode at (a) $\Delta\theta = 0$ and (c) $\Delta\theta = \pi/8$ corresponds to the two triangles in Fig. 9(a) at a bend radius of 9.4 cm. The parallel-polarized core mode at (b) $\Delta\theta = 0$ and (d) $\Delta\theta = \pi/8$ corresponds to the two triangles in Fig. 9(b) at a bend radius of 20.0 cm.

#263392 Received 19 Apr 2016; revised 18 May 2016; accepted 19 May 2016; published 26 May 2016

Figure 9(b) shows the bend losses at different bend relative angles when the bend radius is 20.0 cm. The leakage losses of the two fundamental core modes only change within 7%, as the relative angle increases from 0 to $\pi/8$. It is because the fiber geometry is far from the coupling range between the core mode and tube modes at a bend radius of 20.0 cm. Changing the bend relative angle has almost no effect on the coupling condition. The corresponding mode profiles at relative angles of 0 and $\pi/8$ are shown in Figs. 10(b) and 10(d), respectively. The modes are well confined in the core, and there is not much difference in the mode profile except a rotational shift of $\pi/8$.

6. Conclusion

In this paper, we investigate the bending-induced loss for the two non-degenerate modes in chalcogenide glass negative curvature fibers. The bend loss peaks are induced by the resonant coupling between the core mode and tube modes. It is found that the parallel-polarized mode with respect to the bend direction experiences a higher bend loss than the perpendicular-polarized mode when the coupling occurs between the core mode and the tube mode along the bend direction. The difference between the losses of the two polarization modes is up to a factor of 28 with bend radii down to 10 cm. When coupling occurs between the core mode and the tube mode at 45 degree with respect to the bend direction, the bend losses in the parallel-polarized mode and perpendicular-polarized mode are almost the same. A fiber with a larger tube wall thickness, corresponding to a smaller inner tube diameter, can sustain a smaller bend radius due to the larger index difference between the core mode and tube mode. The bend loss changes by a maximum factor of 12 as the bend direction changes when the bend radius is 9.4 cm. The bend loss only changes by 7% as the bend direction changes when the bend radius is 20.0 cm. Hence, the bend loss is sensitive to the bend direction when coupling occurs between the core mode and tube modes. Overall, a bend loss of 0.2 dB/m at a bend radius of 16 cm, corresponding to 0.2 dB/turn, can be achieved in a chalcogenide negative curvature fiber at a wavelength of 5 μm. We conclude that polarization effects should be considered when designing fibers to withstand bend loss and polarization effect on bend loss.

Our study shows that the bend loss of the two polarization modes in negative curvature fibers can differ significantly. This differential bend loss could be used to make bending sensors [50, 51], in which the bend in the transverse direction is quantified by monitoring the losses in the two polarizations. Hence, negative curvature fibers are a good candidate for use in highly sensitive optical bending sensor systems.

Acknowledgments

This research was supported in part by funds from the Vice Provost for Research at Baylor University. Work at UMBC was supported by the Naval Research Laboratory.

#263392 Received 19 Apr 2016; revised 18 May 2016; accepted 19 May 2016; published 26 May 2016